Chemical and Process Engineering: New Frontiers, 2026, 47(1), e122
DOI: 10.24425/cpe.2026.158120

Electrical and energy study of a volumetric microexpander in an ORC micro power plant

Tomasz Z. Kaczmarczyk, Grzegorz Żywica

Institute of Fluid-Flow Machinery, Polish Academy of Sciences, Fiszera 14, 80-231 Gdańsk, Poland

* **Corresponding author, e-mail:** tkaczmarczyk@imp.gda.pl

Article info:
Received: 11 July 2025
Revised: 21 November 2025
Accepted: 20 January 2026

Abstract
This paper presents the results of an electrovibrational investigation of the expansion unit in a micro-CHP ORC power plant. The study demonstrates that a maximum electrical output of approximately 0.64 kW was achieved in the ORC system at an HFE-7100 flow rate of 0.06 kg/s and a heat source power of 16 kW. It has been determined that, for any given working fluid flow rate, there is an optimal heat source thermal power at which the electrical output of the ORC system reaches its maximum. In contrast, for any preset heat source power and working fluid flow rate, there is an optimal generator load at which the electrical power output of the ORC system is maximised. It has been observed that, irrespective of the working fluid flow rate, changes in thermal power cause the electrical power output of the ORC system to vary along the generator's load line. The research also included vibration measurements, which showed that the operating conditions of the expander unit, including the electrical load on the generator, influenced the vibroacoustic behaviour of the machine.

Keywords
scroll expander, micro-CHP ORC, vibration, HFE-7100

1. INTRODUCTION

Sustainable development (Weerakoon and Assadi, 2024), along with the environment and energy resources, has necessitated the search for ways to improve the efficiency (Ahmed, 2022) of existing industrial systems (Belousov and Ovchinnikov, 2022) or the development of new energy technologies (Weerakoon and Assadi, 2023; Sanaye and Ghaffari, 2023). Therefore, systems are being built to recover waste heat (Zhang et al., 2023b), e.g. from internal combustion engines (Di Battista and Cipollone, 2023), and convert it into electricity, and these are becoming increasingly popular. An example of this is the construction of hybrid systems (Ahmed, 2024) that operate in conjunction with renewable energy sources (RES) (Montazerinejad and Eicker, 2022), thermal energy storage (TES) systems (Kolasiński and Daniarta, 2021), compressed air storage systems (Guan et al., 2024), nuclear power plants (Tauveron et al., 2024), direct-fired hot water boilers (Feng et al., 2024), or conventional energy systems (Kruk-Gotzman et al., 2023). The use of clean hydrogen technologies, including fuel cells (Pielecha and Szwajca, 2024), in the power industry is another example of energy development.

Recently, there has been a strong emphasis on low-temperature heat recovery (Hasan et al., 2022) for the production of cold (González et al., 2023) and electricity (Hossain et al., 2024) in organic Rankine cycle (ORC) systems (Sun and Peng, 2025). The thematic literature shows that studies and analyses of ORC system components (Ma et al., 2022; Zaniewski et al., 2023) include circulating pumps (Kaczmarczyk et al., 2019; Kaczmarczyk, 2024), expansion assemblies (Huo et al., 2022), heat exchangers (Abbas et al., 2022), and the selection of working fluids (Aziz et al., 2024) used in the cycle. In ORC systems, two types of expansion units are used for electricity generation, namely volumetric (Wei et al., 2023) and flow (Witanowski, 2024; Wu et al., 2024), i.e. single-stage (Li et al., 2022a) and multi-stage turbines (Peng et al., 2024a; Wang and Peng, 2023).

Turbines used in ORC systems are of radial-flow (Alshammari et al., 2025; Witanowski et al., 2023c), axial-flow (Kaczmarczyk and Żywica, 2022b; Kupka et al., 2025), or radial-axial-flow (Rusanov et al., 2025; Witanowski et al., 2023b) design. Much of the thermal literature concerns design (Abdalhamid and Eltaweel, 2024; Li et al., 2025) and optimisation (He et al., 2025; Li et al., 2022b) methods for turbines and their components, such as rotors (Lu et al., 2023), blades (Ping et al., 2022; Witanowski et al., 2023a), nozzles (Liaw et al., 2023; Serafino et al., 2023), and stators (Gunawan et al., 2023). In ORC microsystems, where a high pressure ratio (PR) is required at a low flow rate of the working fluid (Daniarta et al., 2022), partial-admission microturbines are used (Włodarski and Piwowarski, 2024; Sun et al., 2024). This group includes Tesla turbines, which have an efficiency of approximately 42% at a power output of around 1.2 kW_e (Zhang et al., 2023c). Similarly, the efficiency of classic microturbines with a power output of up to 3 kW_e ranged from approximately 12% (Colak and Arslan, 2024) to around 43% (Peng et al., 2023). For example, a numerical analysis by Peng et al. (2024b) indicates that the efficiency of a 1.5 kW_e supersonic turbine was approximately 46%. Meanwhile, a study by Sun et al. (2024a) determined that the efficiency of a 0.8 kW_e axial-flow turbine operating in an ORC system with R1233zdE as the working fluid was approximately 36%. In contrast, the efficiency of a single-stage, partial-admission, supersonic impulse ORC turbine with a power output of 1.5 kW_e was approximately 42%.

In the second group, i.e. volumetric expansion units, the most commonly used devices are scroll expanders (Zhen et al., 2024), multi-vane expanders (Daniarta et al., 2024), Wankel expanders (Sprouse, 2024), screw expanders (Mukherjee and Seshadri, 2023), and piston expanders (Gopal and Seshadri, 2022; Wołowicz et al., 2021). Tests of these expansion units are conducted in systems operating with either a single (Kaczmarczyk and Żywica, 2024) or multiple (Ekwonu et al., 2023) expanders under mechanical (Kottapallia and Konijeti, 2022) or resistive (Zhang et al., 2024) load of the generator. The efficiency of volumetric expanders with a power output of up to 3 kW_e reached approximately 50% (Kaczmarczyk and Żywica, 2022a), while the thermal and Carnot efficiencies were 9% and 20%, respectively (Zhang et al., 2023a). For example, a study by Murthy et al. (2022) found that the efficiency of a 0.03 kW_e four-intersecting-vane expander operating in an ORC system with R134a as the working fluid was around 35%.

The paper presents the results of an experimental investigation of a volumetric expansion microunit in an ORC system using the low-boiling fluid methoxy-nonafluorobutane (HFE-7100). The novelty and originality of this work lie in the current–voltage characteristics and vibration measurements of the expansion unit, which are virtually absent from the existing literature. The present work fills a gap in the literature concerning parametric, thermal, flow, and energy analyses, as well as the vibration characteristics of micro-CHP ORC expansion units. The research shows that, for each level of heat source thermal power, there is an optimal generator load at which the electrical power output of the ORC system is maximised. It was determined that, irrespective of the working fluid flow rate and heat source power, the electrical power characteristics are linear and directly proportional to the voltage at the terminals of the expansion microunit's generator.

2. EXPERIMENTAL TEST STAND

Tests of an expansion microunit with a rated power of 1 kW_e were carried out on a specially designed test stand, with a photograph and a measurement diagram shown in Figs. 1 and 2, respectively. The expansion unit consisted of a scroll expander (E15H22N4.25 from Air Squared), a magnetic coupling, and an AB30L generator (WEIPU) supplied by Voltmaster. The technical data for the tested expansion unit are shown in Table 1. A system consisting of two induction modules, each with a rated power of 2×24 kW_e, was used to heat the thermal oil. Only one module of the induction thermal-oil heater was used in the research. The heating device is a prototype unit made to special order and powered by a 3×400 V AC supply, with a maximum power of 24 kW_e. According to the manufacturer (Table 3), the measurement limit error for electrical power supplied from the power grid for a single 24 kW_e module is ± 0.12 kW_e. The heater simulated a low-temperature heat source.

Table 1. Technical parameters of the expansion unit.

Parameter	Unit	Value
Scroll expander		
Nominal power	kW	1.0
Maximum pressure	kPa	1 380
Displacement	cm^3/rev.	12
Maximum speed	rpm	3 600
Maximum inlet temperature	°C	175
Expansion ratio	–	3.5
AC generator		
Rated power	kW	2.4
Maximum rotational speed	rpm	3 000
Rated voltage	V	240
Maximum current	A	10

A specification of the primary components used to construct the test rig, along with their technical parameters, is provided in Table 2.

The heat source allowed the thermal oil to be heated up to 400 °C, with the temperature adjustable in increments of 0.1 °C. The flow rate of the thermal oil was controlled by varying the rotational speed of the pump's electric drive using a frequency converter.

Figure 1. Test rig for the expansion microunit: 1 – scroll expander, 2 – clutch, 3 – generator, 4 – generator load system, 5 – heat source.

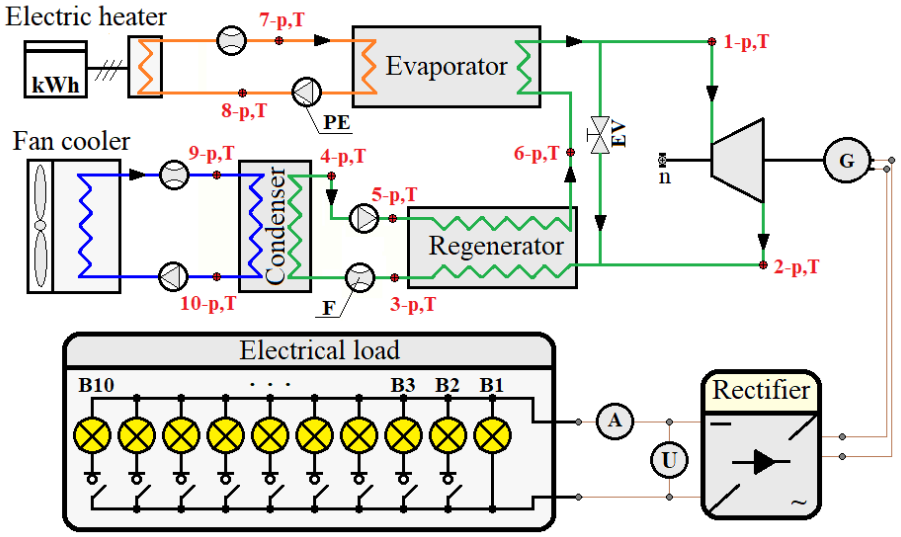

Figure 2. Measurement diagram of the ORC system with a 1 kW scroll expander: PE – pumping engine, F – flowmeter, n – rotational speed measurement system, EV – expansion valve, B – electrical bulb, A – ammeter, U – voltmeter, G – generator, T – temperature measurement, p – pressure measurement, 1–10 – state points.

Table 2. Main components of the test rig (Kaczmarczyk and Żywica, 2022b).

Component name	Type/model	Parameters	Producer
Evaporator	plate heat exchanger	$A = 4.1$ m^2	Secespol
Regenerator	shell-and-tube heat exchanger	$A = 2.3$ m^2	Secespol
Condenser	plate heat exchanger	$A = 3.2$ m^2	Secespol
Heat source	–	2×24 kW$_e$	prototype
Fan cooler	TDR 01 06 53-C	50 kW$_t$ $p_{max} = 6$ bar	GEA
Pumping engine (HFE-7100)	4030–710-B-DM	$p_{max} = 12$ bar $m_{max} = 20$ l/min	Scherzinger
Pumping engine (ethylene glycol)	25 POeC100 Mega	$p_{max} = 11$ bar $m_{max} = 11$ m^3/h	LFP Leszno
Pumping engine (thermal oil)	L018-03R-NF-00-T	$p_{max} = 16$ bar $m_{max} = 36.3$ m^3/h	TopGear

The same method was used to control the flow rate of both the working fluid and the ethylene glycol solution, namely by adjusting the pump rotational speed through regulation of the supply voltage frequency to the pump drives (electric motors) using a frequency converter. A specification of the sensors and measuring equipment installed on the test rig is provided in Table 3. The thermal oil, heated to the set temperature, was directed to the evaporator, where the working fluid was evaporated. Once the appropriate operating parameters were achieved, the working fluid vapour was directed via a bypass to the regenerator and then to the condenser. Heat from the condenser was dissipated into the environment using a fan cooler with a nominal capacity of 50 kW$_t$. The condensed fluid was first directed to the regenerator, where it was preheated, and then to the evaporator. The low-boiling fluid vapour, once the required pressure was achieved at the set flow rate, was directed to the inlet of the expansion unit. The expansion unit comprised a scroll expander connected to the generator via a clutch. The generator was connected to a specially designed resistive (R-type) load system. The load system was equipped with an AC/DC converter, to which a set of 10 DC bulbs was connected. The rated power of each bulb was 200 W$_e$. Each bulb (electrical receiver) was fitted with an on/off switch, allowing the generator load to be adjusted from 200 W$_e$ to 2,000 W$_e$.

The combined uncertainty of the electric output power of the AC/DC converter in the ORC system was calculated using the square error propagation rule, based on the following relationship:

$$\delta N_e = \sqrt{\left(\left|\frac{\delta N_e}{\delta u}\right| \delta u\right)^2 + \left(\left|\frac{\delta N_e}{\delta i}\right| \delta i\right)^2} \tag{1}$$

The output power of the ORC system was calculated using the following relationship:

$$N_e = U \cdot I \tag{2}$$

where U is the DC voltage [V] and I is the current [A].

Based on Table 3, the limit (maximum) errors of DC voltage and current measurements were estimated to be ±1.5 V and ±0.08 A, respectively. For a nominal power of the scroll expander of 1 kW (Table 1) and a maximum voltage at the generator terminals of 240 V (Table 1), the load current is 4.17 A, and the uncertainty of the electrical output power of the ORC system, determined from Eq. (1), is 1000 ± 20.2 W_e. In contrast, at the maximum power of the scroll expander of 1 kW and the maximum load current of the generator of 10 A (Table 3), the voltage is 100 V. The uncertainty in determining the output power of the ORC system is then 1000 ± 17.0 W_e. Based on data provided by the manufacturer of the Coriolis flow meter, the calculated uncertainty of the working-medium flow rate measurement over the range of 30–60 g/s was ±0.5 g/s. In the ORC system, HFE-7100 was used as the working fluid. The fluid was selected on the basis of thermodynamic and energy considerations, taking into account environmental and safety aspects. HFE-7100 is a dry fluid (Fig. 3) that protects the flow components of the expansion unit against erosion.

HFE-7100 is a low-boiling liquid with a boiling point of approximately 61 °C at atmospheric pressure and a reference temperature of 25 °C. Further information on the physicochemical properties of HFE-7100 can be found in reference

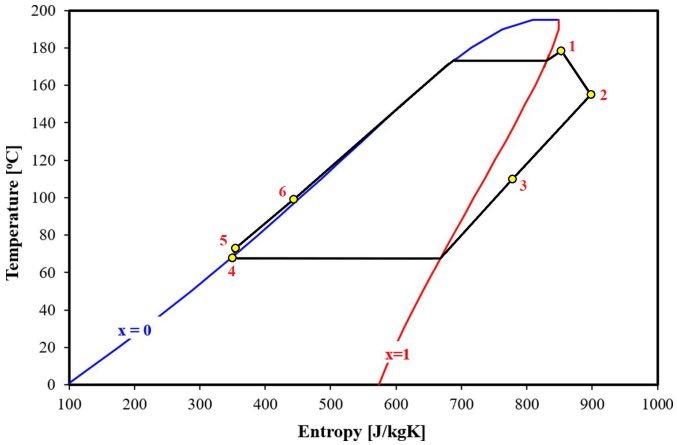

Figure 3. T–s diagram of the scroll expander test cycle.

(Liaw et al., 2023). HFE-7100 is also non-flammable, non-explosive, non-mutagenic, and non-toxic. The global warming potential (GWP) of this fluid is approximately 320, and its ozone depletion potential (ODP) is zero.

3. RESEARCH PROCEDURES AND METHODOLOGY

The research procedure involved setting an appropriate heat source power and working fluid flow rate, and achieving stable operating parameters for the ORC system. The research was conducted at six different heat source power levels. The minimum preset power of the heat source was 8 kW_t, which was increased in 2 kW_t increments up to

Table 3. List of control and measurement apparatus.

Device/sensor (type/mode)	Range	Accuracy
K-type thermocouple, Class 1 tolerance, manufactured by CZAKI Thermo-Product	–40–600 °C	±1.5 °C*A)
Pressure transducer, manufactured by Trafag (NAH 8253)	0–1 600 kPa(a)	±0.15% of full scale
Pressure transducer, manufactured by Trafag (NAH 8253)	0–400 kPa(a)	±0.15% of full scale
Smart differential pressure transmitters manufactured by Aplisens (APR-2000 ALW)	–160–200 kPa	±0.10% of full scale
Smart differential pressure transmitters manufactured by Aplisens (APR-2200 ALW)	–16–16 kPa	±0.10% of full scale
Smart differential pressure transmitters manufactured by Aplisens (APR-2200 ALW)	–180–200 kPa	±0.10% of full scale
Smart differential pressure transmitters manufactured by Aplisens (APR-2200 ALW)	0–250 kPa	±0.10% of full scale
Coriolis mass flowmeter manufactured by Siemens (Sitrans FC Massflo Mass 2100)	0–5 600 kg/h	±0.1% of the measured value
Prototype rotational speed measurement device (based on electromagnetic induction), custom-built (M1 TG-3)	0–300 Hz	±1 rpm
Prototype electrical power measurement system, custom-built (M2 TG-3)	0–16 A DC 0–300 V DC 0–2 × 24 kW	±0.5% of full scale ±0.5% of full scale ±0.5% of the power

*A) – the maximum measurement error of the thermocouple, according to the PN-EN 60584 standard

a maximum of 18 kW_t (Fig. 4). The range of heat source power tested corresponds to that of gas boilers installed in single-family houses. Tests were carried out for low-boiling working medium flow rates of up to 60 g/s.

At the minimum heat source power, superheating of the methoxy-nonafluorobutane fluid occurred only at a flow rate of 20 g/s. In contrast, at a heat source power of 18 kW_t, the minimum flow rate of the working fluid was 50 g/s. This was due to the temperature of the low-boiling fluid being above the design temperature of the ORC system and the critical point of the HFE-7100. Hence, the ranges of variation in the flow rate of the working fluid at the set heat source power were determined by the possibility of achieving superheating of the working fluid while ensuring the safe operation of the system.

Once stable operating parameters were achieved for the ORC system at a constant and preset heat source power and flow rate, the fluid vapour was directed to the inlet of the scroll expander. The start-up of the expansion unit took place with a maximum load of 10 bulbs, which was gradually reduced. The minimum load to prevent the expansion unit from diverging was a bulb with a rated power of 200 W_e.

4. RESULTS AND DISCUSSION

Below are the performance characteristics of the expansion unit, illustrating the effect of rotational speed (Section 4.1) and the load voltage and current of the expansion unit (Section 4.2) on the electrical power output of the ORC system. Section 4.3 presents the vibration measurements of the expansion unit.

4.1. The effect of rotational speed

Fig. 5a shows that, at a constant working fluid flow rate of 20 g/s, regardless of the heat source power value, the electrical output power of the ORC system was approximately 150 W_e. It was observed that, with a heat source power of 8 kW_t, the maximum electrical power was achieved at a rotational speed of approximately 1 650 rpm. In contrast, with a heat source power of 10 kW_t, the maximum power was achieved at an expander rotational speed of approximately 1 800 rpm. Hence, for heat source powers of 8 kW_t and 10 kW_t, the optimum generator loads were approximately 4.1 Ω and 5.5 Ω, respectively. The voltage at the generator terminals was directly proportional to the expander's rotational speed and increased as the speed increased (Fig. 5b). It was observed that the average voltage at the generator terminals was independent of the heat source power.

When the flow rate of the working fluid was 30 g/s, a maximum electrical output power of approximately 300 W_e was obtained at a heat source power of 14 kW_t (Fig. 6a). The optimum generator load for this power value was approximately 5.5 Ω, achieved at an expander rotational speed of around 2 000 rpm. In contrast, at power levels of 10 kW_t and 12 kW_t, the maximum electrical output power was 280 W_e. The maximum electrical power for this case was achieved at a rotational speed of 1 900 rpm and a load of approximately 4.5 Ω. The voltage at the generator terminals increased as the load decreased, leading to an increase in the expander rotational speed (Fig. 6b). For a low-boiling fluid flow rate of 40 g/s (Fig. 7a), it was observed that the electrical output power of the ORC system increased as the thermal power of the heat source rose.

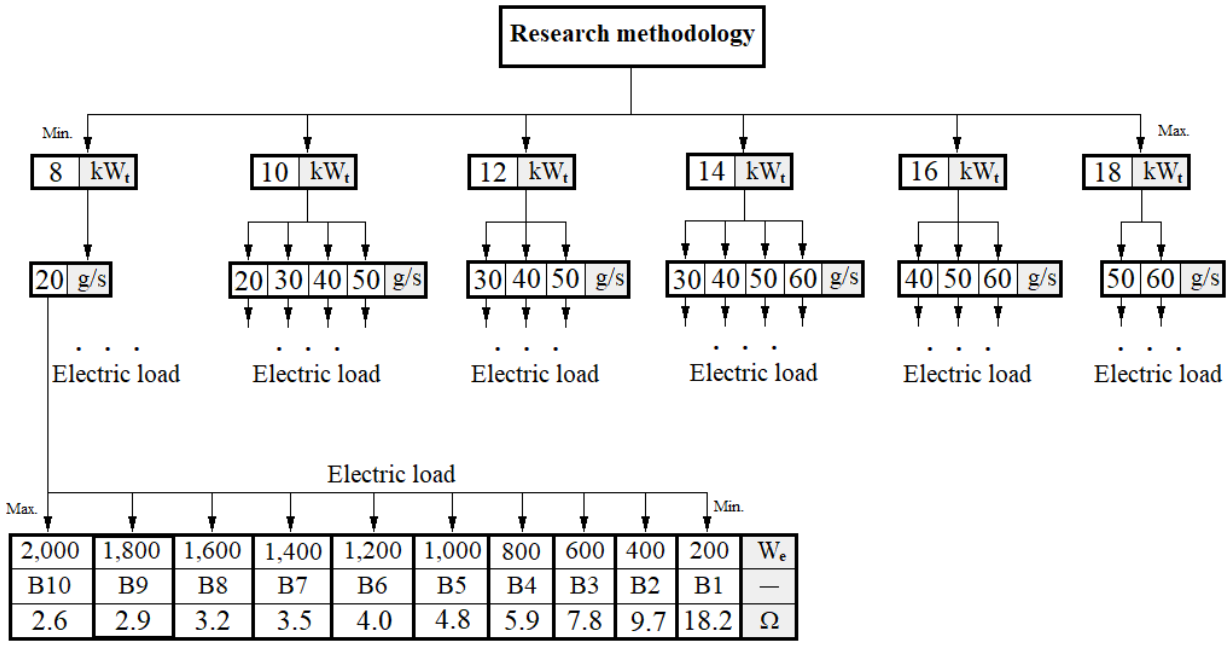

Figure 4. Research procedure used for the scroll expander.

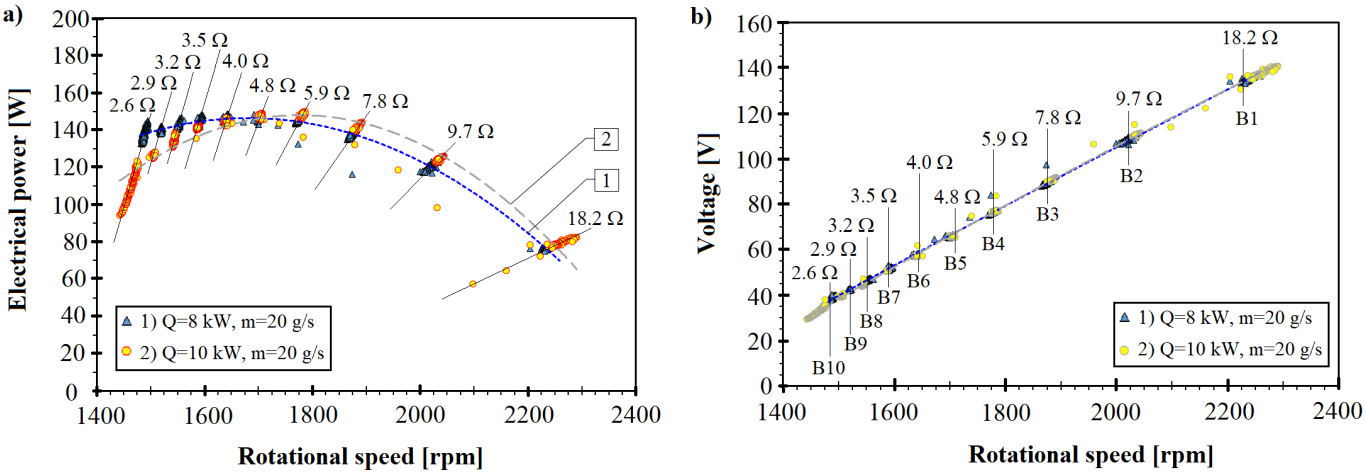

Figure 5. Performance characteristics of the expander at a working medium flow rate of 20 g/s.

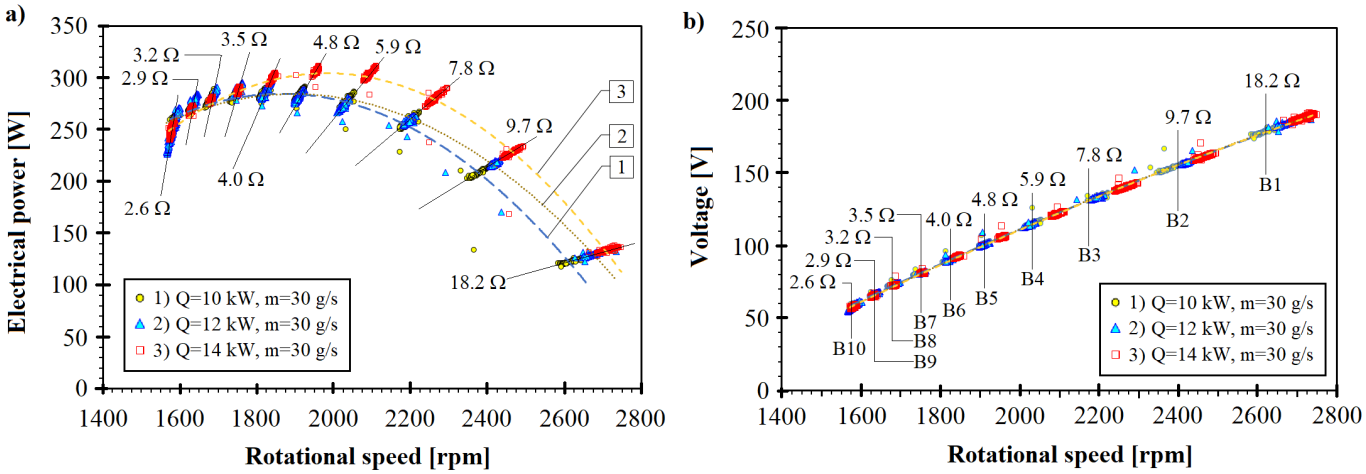

Figure 6. Performance characteristics of the expander at a working medium flow rate of 30 g/s.

For heat source powers of 10 kW_t, 12 kW_t, 14 kW_t, and 16 kW_t, maximum electrical powers of approximately 380 W_e, 415 W_e, 420 W_e, and 430 W_e were obtained, respectively.

In contrast, the resistance values loading the generator for these power levels were 3.8 Ω, 4.0 Ω, 4.1 Ω, and 4.8 Ω, respectively. The rotational speeds at which the maximum electrical output powers of the system were obtained increased with the increasing heat source power (10 kW_t, 12 kW_t, 14 kW_t, and 16 kW_t) and were 1 970 rpm, 2 040 rpm, 2 070 rpm, and 2 150 rpm, respectively. As with the working fluid flow rates of 20 g/s and 30 g/s, the average voltage at the generator terminals increased linearly with the increasing expander rotational speed (Fig. 7b). When the heat source power was 10 kW_t, the maximum electrical power was approximately 400 W_e (Fig. 8a). When the heat source power was increased by 20%, 40%, 60%, and 80% from 10 kW_t (i.e., to 18 kW_t), the maximum electrical output power of the ORC system increased from 400 W_e by 20%, 25%, 35%, and 40%, respectively, reaching 560 W_e.

This means that as the thermal power increased, the increments in electrical energy became progressively smaller. In contrast, the optimum load values for the power maxima increased with the increasing thermal power of the heat source and were 3.3 Ω, 3.7 Ω, 3.8 Ω, 3.9 Ω, and 4.0 Ω, respectively (Fig. 8b).

When the working fluid flow rate was 60 g/s, a maximum electrical power of approximately 640 W_e was achieved at a thermal power of 16 kW_t, while a minimum power of approximately 560 W_e was recorded at a thermal power of 14 kW_t (Fig. 9a).

Hence, it can be observed that, for a given working fluid flow rate, there is an optimum heat source power at which the electrical output power of the ORC system reaches its maximum. The optimum generator load values for heat source powers of 14 kW_t, 16 kW_t, and 18 kW_t were 4.5 Ω, 4.7 Ω, and 4.7 Ω, respectively (Fig. 9b). Optimum loads were achieved at expander rotational speeds of 2 150 rpm, 2 250 rpm, and 2 225 rpm, respectively.

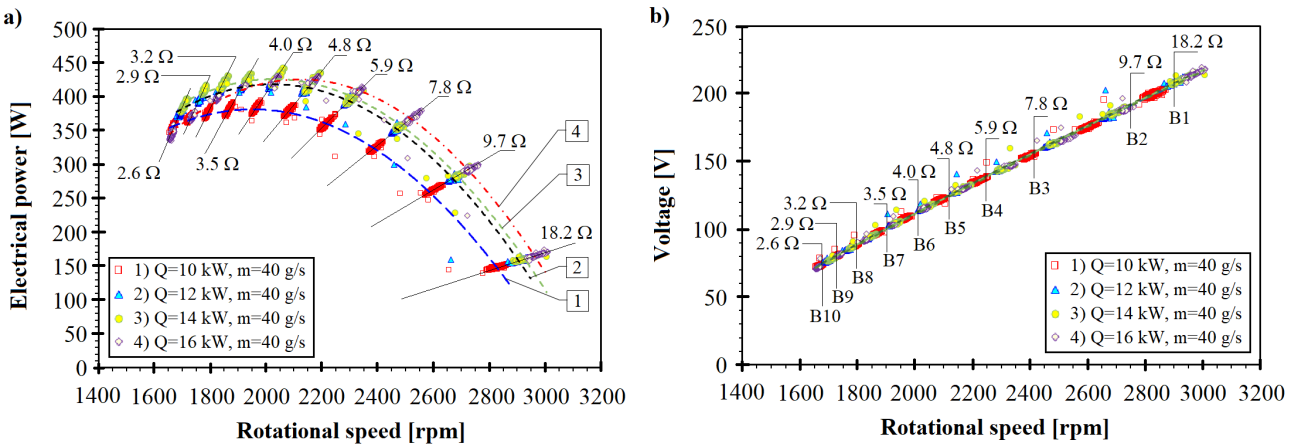

Figure 7. Performance characteristics of the expander at a working medium flow rate of 40 g/s.

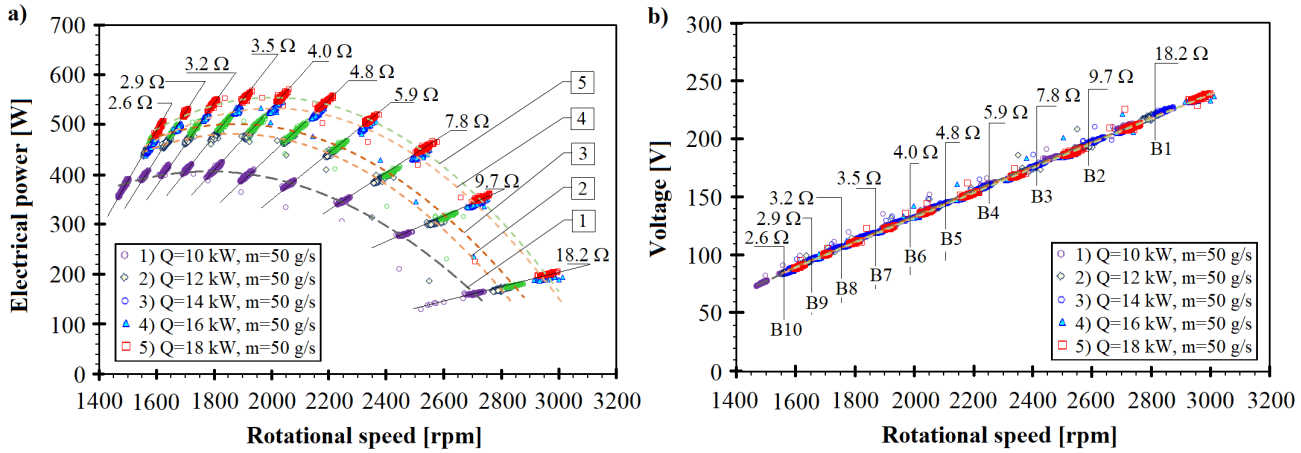

Figure 8. Performance characteristics of the expander at a working medium flow rate of 50 g/s.

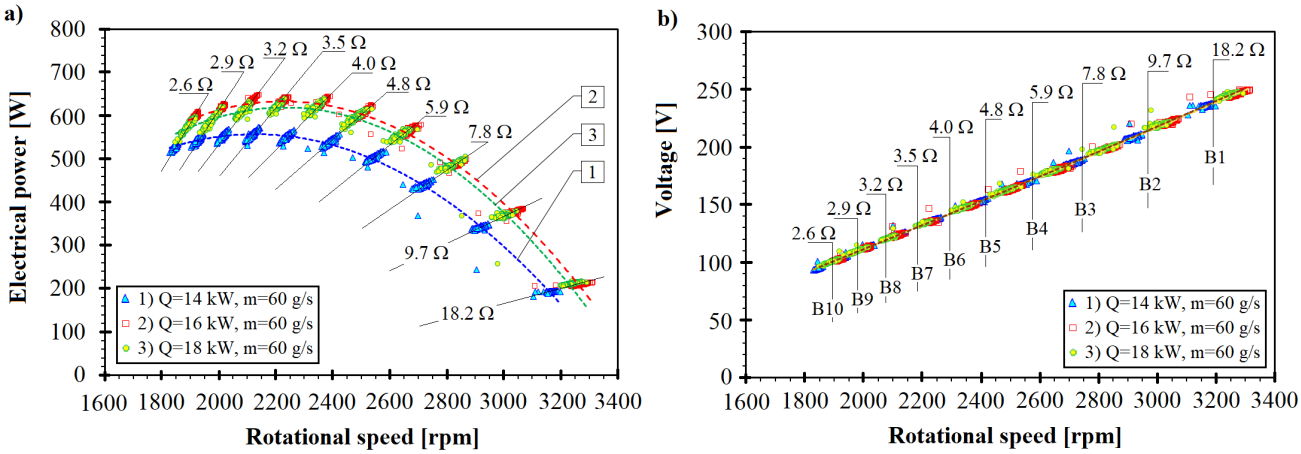

Figure 9. Performance characteristics of the expander at a working medium flow rate of 60 g/s.

4.2. The effect of generator load

It was found that, at a flow rate of 20 g/s and the expander generator's optimum load, the current and voltage at the expander terminals for a heat source power of 8 kW_t were approximately 2.5 A and 60 V, respectively.

In contrast, for a heat source power of 10 kW_t, the optimum values for current (Fig. 10a) and voltage (Fig. 10b) were 2.1 A and 72 V, respectively.

For a flow rate of 30 g/s and heat source powers of 10 kW_t and 12 kW_t, the average current (Fig. 11a) and voltage (Fig. 11b) values for maximum electrical output power were 3.0 A and 94 V, respectively.

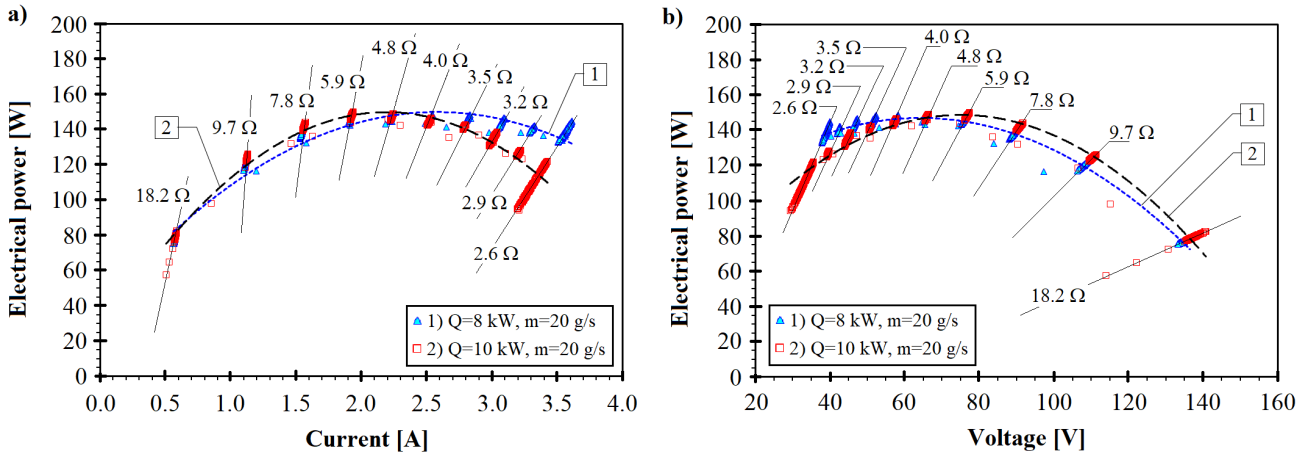

Figure 10. Performance characteristics of the expander at a working medium flow rate of 20 g/s.

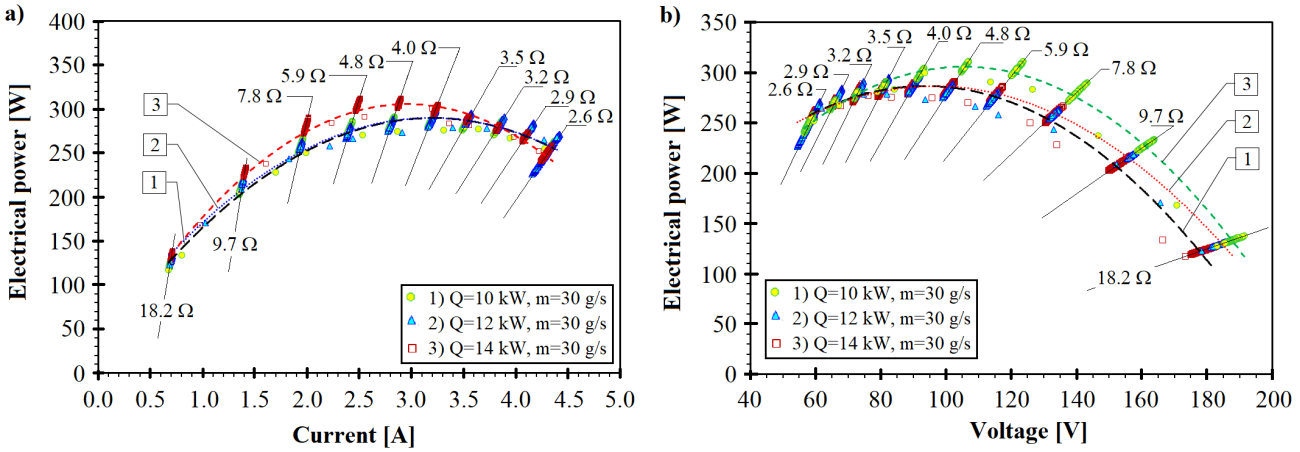

Figure 11. Performance characteristics of the expander at a working medium flow rate of 30 g/s.

Fig. 12a shows that for thermal powers of 10 kW_t, 12 kW_t, 14 kW_t, and 16 kW_t, the voltage values were 98 V, 112 V, 117 V, and 127 V, respectively. In contrast, at maximum electrical output power, the generator load currents decrease as the thermal power of the heat source increases. For thermal powers ranging from 10 kW_t to 16 kW_t (Fig. 12b), the optimum current values were 3.9 A, 3.7 A, 3.6 A, and 3.4 A, respectively.

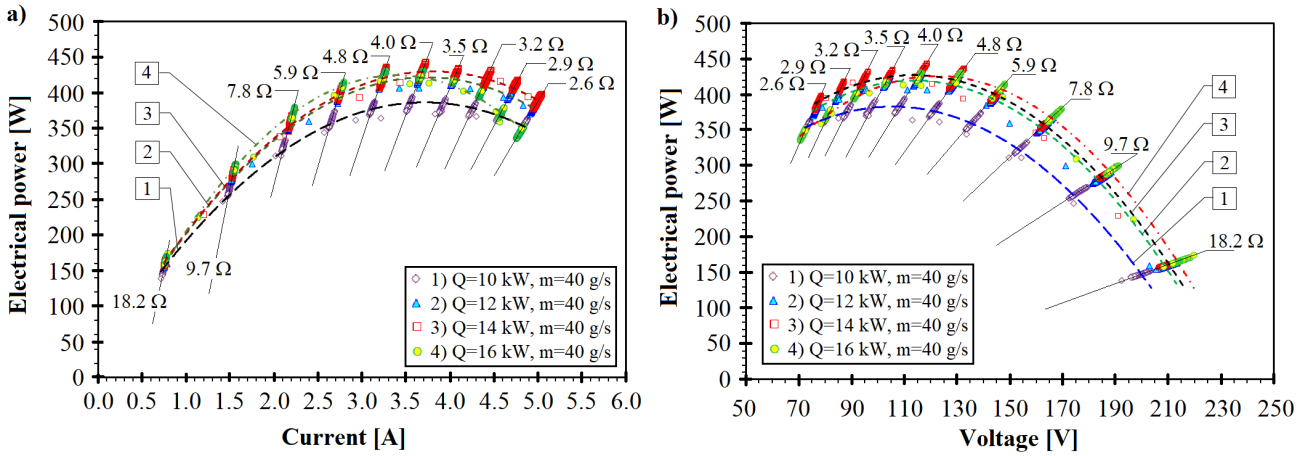

Figure 12. Performance characteristics of the expander at a working medium flow rate of 40 g/s.

It was observed that, for a flow rate of 50 g/s, the current, regardless of the heat source power value, was approximately 4–4.1 A (Fig. 13b). In contrast, the voltage values at the generator terminals increased as the thermal power of the heat source increased.

For thermal powers of 10 kW_t and 12 kW_t, the optimum voltage values were 98 V and 117 V, respectively. In contrast, for heat source powers of 14 kW_t, 16 kW_t, and 18 kW_t, the voltages at the generator terminals were 127 V, 132 V, and 135 V, respectively.

When the working fluid flow rate was 60 g/s, the same currents of approximately 4.7 A were obtained at maximum electrical output powers for thermal powers of 16 kW_t and 18 kW_t (Fig. 14b). In contrast, the average voltage values were 135 V and 133 V, respectively. For a thermal power of 14 kW_t at maximum electrical power output, the average voltage and current values were 123 V and 4.5 A, respectively. It follows from the above that, irrespective of the flow rate of the low-boiling fluid, for a given generator load, an increase in thermal power causes the power to move along the load line.

4.3. Vibration measurements of the expansion unit

Based on the analysis of the vibration spectra of the expander and generator shown in Figs. 15–18, it can be concluded that the vibration distributions were rather chaotic.

The expander tests also involved vibration measurements conducted under various operating conditions. Such measurements allow for the assessment of the dynamic condition of a fluid-flow machine and facilitate early detection of various types of faults, such as bearing or rotor damage. Vibrodiagnostic testing involved measuring absolute vibrations on the bodies of the expander and generator. The measured quantity was the root mean square (RMS) value of the vibration velocity (V_{rms}). In addition to measuring the overall V_{rms} value, the vibration spectrum was also recorded over the range of 1 Hz to 1,600 Hz. The figures below (Figs. 15–18) present selected measurement results obtained at four rotor speeds (ranging from 2,028 rpm to 2,364 rpm) and various generator loads (from 550 W to 1,150 W). The measurement results confirm that a char-

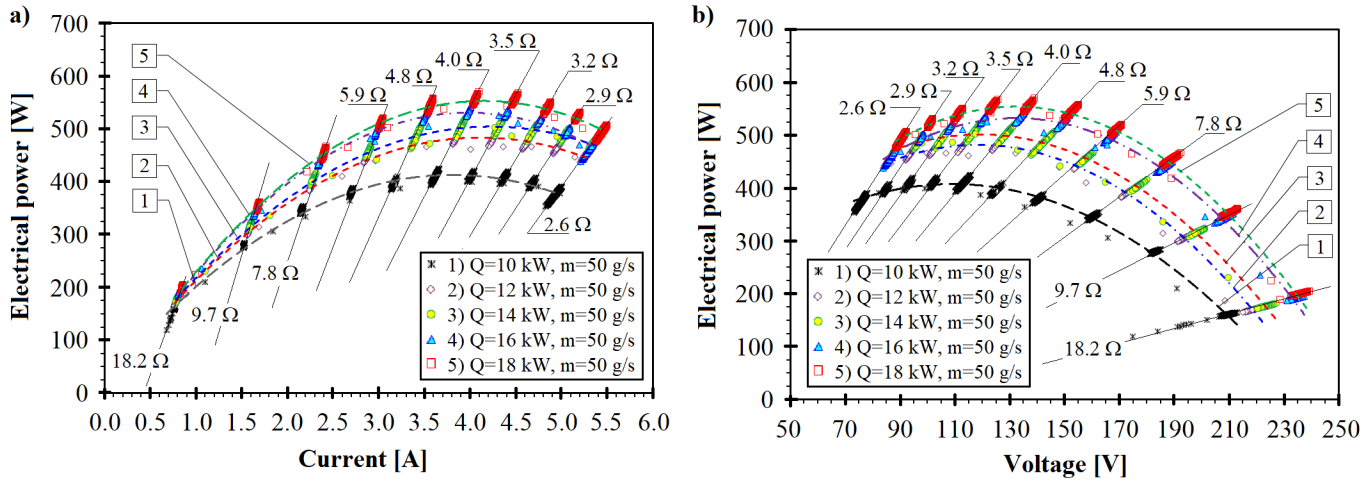

Figure 13. Performance characteristics of the expander at a working medium flow rate of 50 g/s.

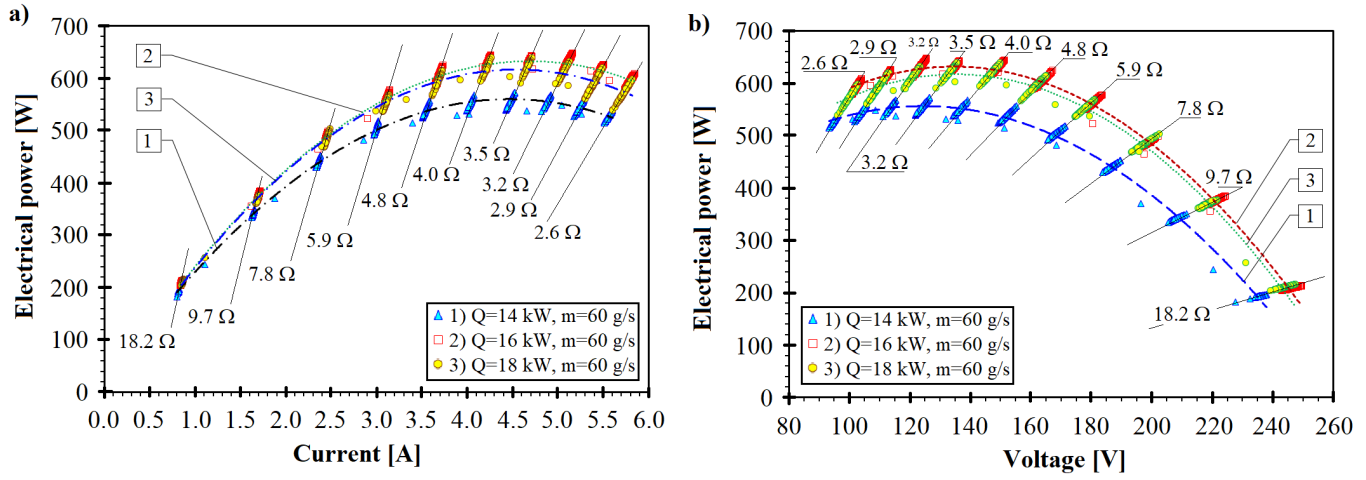

Figure 14. Performance characteristics of the expander at a working medium flow rate of 60 g/s.

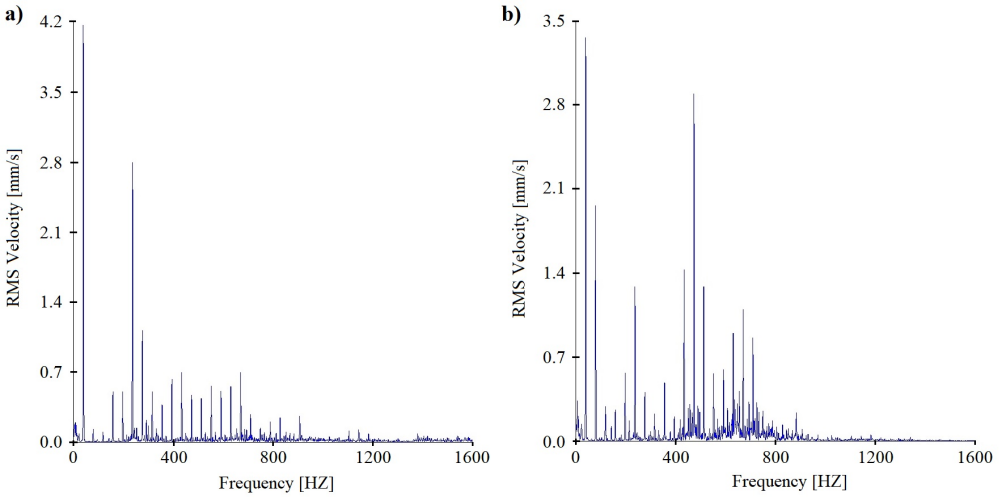

Figure 15. Frequency distributions of vibration velocity measured on the scroll expander housing (a) and the generator (b) at a rotational speed of 2 028 rpm and a receiver load power of 550 W.

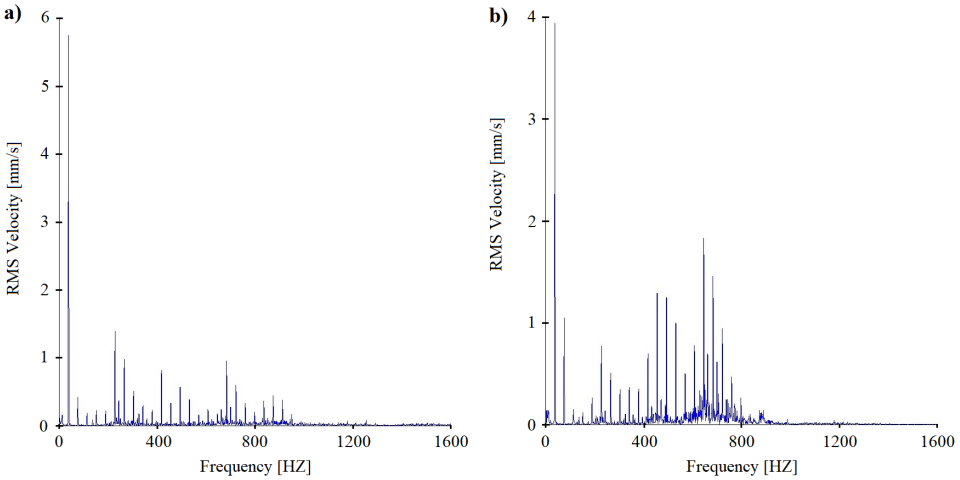

Figure 16. Frequency distributions of vibration velocity measured on the scroll expander housing (a) and the generator (b) at a rotational speed of 2 172 rpm and a receiver load power of 750 W.

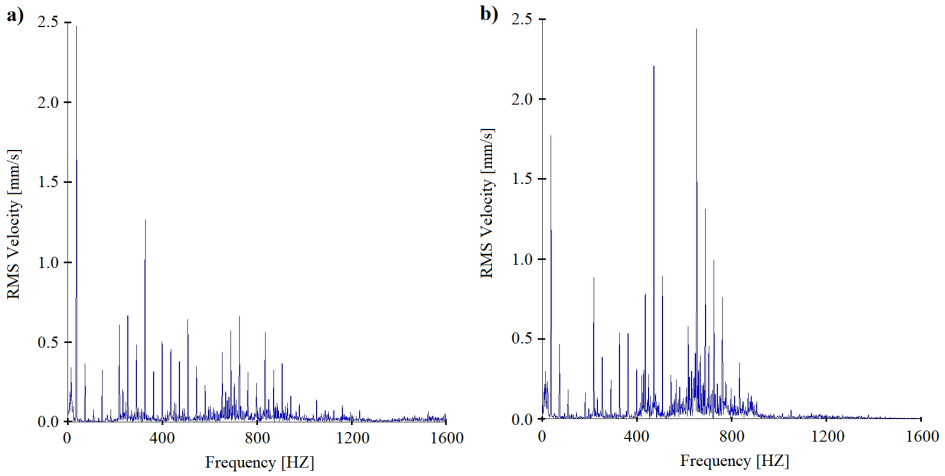

Figure 17. Frequency distributions of vibration velocity measured on the scroll expander housing (a) and the generator (b) at a rotational speed of 2 280 rpm and a receiver load power of 950 W.

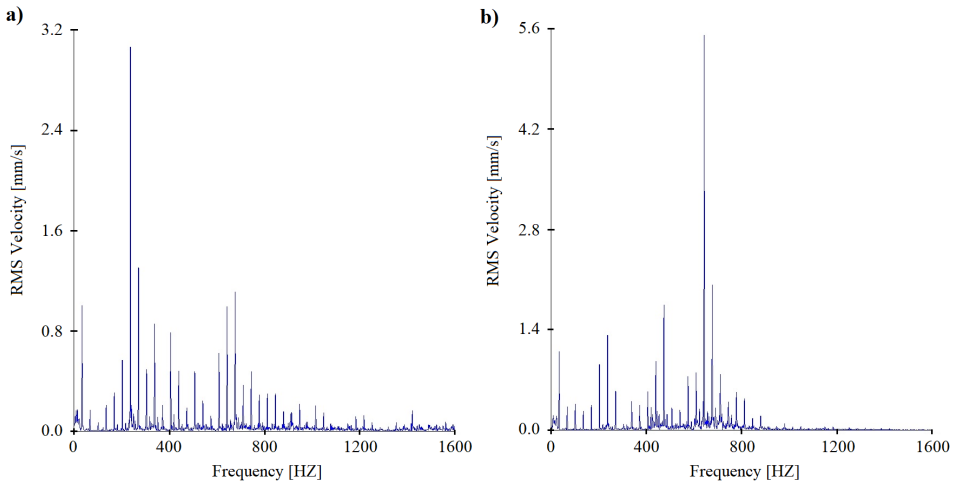

Figure 18. Frequency distributions of vibration velocity measured on the scroll expander housing (a) and the generator (b) at a rotational speed of 2 364 rpm and a receiver load power of 1,150 W.

acteristic feature of the tested scroll expanders is irregular knocking operation, as evidenced by numerous spectral lines visible in the frequency distributions of vibration velocity.

To facilitate the interpretation of the results, a histogram was prepared (Fig. 19) showing the overall V_{rms} vibration levels recorded at different generator loads. It can generally be stated that the vibration level of the expansion unit varied according to the power of the connected electrical receivers. A certain tendency towards an increase in the high-frequency components at lower power levels of the energy receivers can be discerned, but it was not observed in all cases studied.

However, it is difficult to discern a clear trend, as the analysed values initially decreased and then increased. Similar trends were observed for both the generator and the expander. However, the fluctuations in the overall vibration level were not large, ranging from 3.77 mm/s for the expander at a power of 750 W to 7.35 mm/s for the generator at a power of 550 W. It can, however, be noted that the lowest vibration levels of both the generator and the expander were observed at a receiver power of 750 W (at a speed of 2 172 rpm). The operation of the expander and electric generator unit can therefore be regarded as most stable within this load range. No signs of damage to the expander unit were detected based on the vibration measurements.

5. CONCLUSIONS

The research on a 1 kW scroll expander in an ORC system shows that, irrespective of the heat source power and working fluid flow rate, the voltage at the generator terminals increases as the generator load decreases. It was determined that, for each thermal power level of the heat source, there were optimum values of the working fluid flow rate and the generator's electrical load at which the electrical output power of the ORC system reached its maximum. It was found that, for each heat source power level, there was an optimum rotational speed of the scroll expander at which the electrical output power of the system reached its maximum.

The research conducted indicates that, for heat source powers ranging from 8 to 18 kW_t and methoxy-nonafluorobutane flow rates between 20 and 60 g/s, a maximum electrical output power of approximately 640 W_e was achieved at a thermal power of 16 kW_t and a working fluid flow rate of 60 g/s. The research conducted also confirmed that the scroll-type volumetric expander is a highly flexible expansion device. During the research conducted, it operated properly across a wide range of heat source power and working fluid flow rates, as well as under different generator loads, enabling the conversion of thermal energy into electrical energy.

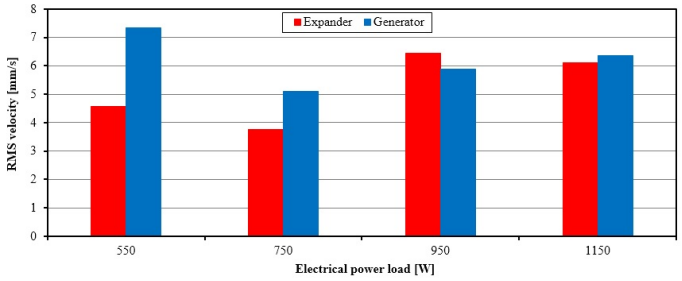

Figure 19. Overall vibration levels of the expander and generator in relation to the generator load.

The research shows that for HFE-7100 flow rates of 20 g/s and 30 g/s, the maximum electric output power of the ORC system was approximately 150 ± 6.2 W_e, obtained for generator loads of 4.1 Ω and 5.5 Ω and heat source powers of 8 kW_t and 10 kW_t, respectively. In contrast, for a working-medium flow rate of 30 g/s, the maximum electrical power of approximately 280 ± 10.0 W_e was obtained at a heat source power of 14 kW_t and a generator load of 4.5 Ω. At an HFE-7100 flow rate of 40 g/s, the maximum output power of the system was approximately 430 ± 11.5 W_e, obtained at an expander rotational speed of 2 150 rpm and a generator load of 4.8 Ω with a heat source power of 16 kW_t, respectively. When the flow rate of the low-boiling fluid was 50 g/s, the maximum electrical power produced by the expansion unit was 560 ± 13.1 W_e, obtained at a heat source power of 18 kW_t and a generator load of approximately 4.0 Ω. A similar maximum electrical output power of the ORC system was obtained at an HFE-7100 flow rate of 60 g/s, with an expander generator load of approximately 4.7 Ω and a heat source power of 16 kW_t.

Vibration measurements indicate that a notable drawback of this type of expander is its high vibration level, which results in relatively noisy operation. The research shows that the recorded vibration level of the expansion unit ranged from 3.77 mm/s to 7.35 mm/s, measured when the expander generator was connected to receivers with rated powers of 750 W and 550 W, respectively. This drawback can be significantly mitigated through the appropriate selection of the support system and enclosure, i.e. by ensuring adequate vibration and acoustic isolation.

ACKNOWLEDGEMENTS

This research was conducted as part of the project entitled "Preliminary studies of thermodynamic cycles with low-boiling 73DE fluid" (2023/07/X/ST8/01193), funded by the National Science Centre in Poland.

SYMBOLS

I	current, A
m	mass flow rate, kg/s
n	rotational speed, rpm
N	power, W
R	resistance, Ω
T	temperature, °C
U	voltage, V
V_{rms}	root mean square of the vibration velocity

Subscripts

e	electrical
t	thermal

Abbreviations

AC	alternating current
DC	direct current
ORC	organic Rankine cycle
PR	pressure ratio
RES	renewable energy sources
TES	thermal energy storage
WHR	waste heat recovery

REFERENCES

Abbas W.K., Baumhögger E., Vrabec J., 2022. Experimental investigation of organic Rankine cycle performance using alkanes or hexamethyldisiloxane as a working fluid. *Energy Convers. Manage.: X*, 15, 100244. DOI: 10.1016/j.ecmx.2022.100244.

Abdalhamid A.M.K., Eltaweel A., 2024. Design and analysis of a single-stage supersonic turbine with partial admission. *Energy*, 309, 133100. DOI: 10.1016/j.energy.2024.133100.

Ahmed A.M., 2022. Assessment of the thermal efficiency of subcritical power generation cycles using environmentally friendly fluids at various heat source temperatures. *Energy Sci. Eng.,* 10, 4768–4781. DOI: 10.1002/ese3.1307.

Ahmed A.M., 2024. Thermal efficiency investigation for organic Rankine cycle and trilateral flash cycle using hydrofluoroether working fluids. *Results Eng.*, 21, 101648. DOI: 10.1016/j.rineng.2023.101648.

Alshammari F., Alshammari A.S., Alzamil A., 2025. Advanced energy conversion strategies using multistage radial turbines in Organic Rankine Cycles for low-grade heat recovery. *Case Stud. Therm. Eng.,* 69, 106034. DOI: 10.1016/j.csite.2025.106034.

Aziz F., Kamal S.M., Perl M., Chetry A., 2024. Increasing the load carrying capacity of hollow rotating disks by applying rotational autofrettage. *Eur. J. Mech. A. Solids*, 105, 105231. DOI: 10.1016/j.euromechsol.2024.105231.

Belousov A.E., Ovchinnikov E.S., 2022. Mathematical modeling of the operation of an expander-generator pressure regulator in non-stationary conditions of small gas pressure reduction stations. *Mathematics*, 10, 393. DOI: 10.3390/math10030393.

Colak A.B., Arslan O., 2024. Numerical analysis-based performance assessment of the small-scale organic Rankine cycle turbine design for residential applications. *Therm. Sci. Eng. Prog.*, 51, 102626. DOI: 10.1016/j.tsep.2024.102626.

Daniarta S., Imre A.R., Kolasiński P., 2022. Thermodynamic efficiency of subcritical and transcritical power cycles utilizing selected ACZ working fluids. *Energy*, 254, Part A, 124432. DOI: 10.1016/j.energy.2022.124432.

Daniarta S., Kolasiński P., Imre A.R., Sowa D., 2024. Artificial intelligence-driven performance mapping: A deep learning-based investigation of a multi-vane expander in retrofitted organic Rankine cycle. *Energy Convers. Manage.,* 315, 118763. DOI: 10.1016/j.enconman.2024.118763.

Di Battista D., Cipollone R., 2023. Waste energy recovery and valorization in internal combustion engines for transportation. *Energies*, 16, 3503. DOI: 10.3390/en16083503.

Ekwonu M.C., Kim M., Chen B., Nasir M.T., Kim K.C., 2023. Dynamic simulation of partial load operation of an Organic Rankine Cycle with two parallel expanders. *Energies*, 16, 519. DOI: 10.3390/en16010519.

Feng Y.-Q., Xu K.-J., Liu Z.-X., Yu H.-S., Hung T.-C., He Z.-X., 2024. Construction and preliminary test of a biomass-fired organic Rankine cycle system for heat and power system. *Energy*, 308, 133021. DOI: 10.1016/j.energy.2024.133021.

González J., Llovell F., Garrido J.M., Quinteros-Lama H., 2023. A study of the optimal conditions for organic Rankine cycles coupled with vapour compression refrigeration using a rigorous approach based on the Helmholtz energy function. *Energy*, 285, 129554. DOI: 10.1016/j.energy.2023.129554.

Gopal V.V., Seshadri S., 2022. Effect of cut-off and compression ratio on the isentropic efficiency during off-design and part-load operations of a Wankel rotary steam expander used for small scale cogeneration. *Appl. Therm. Eng.*, 207, 118212. DOI: 10.1016/j.applthermaleng.2022.118212.

Guan Y., Li W., Zhu Y., Wang X., Zhang Y., Chen H., 2024. Energy loss analysis in two-stage turbine of compressed air energy storage system: effect of varying partial admission ratio and inlet pressure. *Energy*, 305, 132214. DOI: 10.1016/j.energy.2024.132214.

Gunawan G., Permana D.I., Soetikno P., 2023. Design and numerical simulation of radial inflow turbine of the regenerative Brayton cycle using supercritical carbon dioxide. *Results Eng.*, 17, 100931. DOI: 10.1016/j.rineng.2023.100931.

Hasan A., Mugdadi B., Al-Nimr M.A., Tashtoush B., 2022. Direct and indirect utilization of thermal energy for cooling generation: a comparative analysis. *Energy*, 238, Part C, 122046. DOI: 10.1016/j.energy.2021.122046.

He S., Tong Z., Tong S., Chen K., Cao X.E., 2025. Collaborative optimization of turbo-expander impellers and guide vanes to mitigate flow-induced vibrations. *Phys. Fluids,* 37, 035178. DOI: 10.1063/5.0257754.

Hossain M.S., Sultan I., Phung T., Kumar A., 2024. An optimum design for a fast-response solenoid valve: application to a limaçon gas expander. *Dynamics*, 4, 457–474. DOI: 10.3390/dynamics4020024.

Huo E., Xin L., Wang S., 2022. Thermal stability and pyrolysis mechanism of working fluids for organic Rankine cycle: a review. *Int. J. Energy Res.,* 46, 19341–19356. DOI: 10.1002/er.8518.

Kaczmarczyk T.Z., 2024. Experimental research of a pumping engine in a micro-ORC system with a low-boiling medium. *Arch. Thermodyn.*, 45, 125–140. DOI: 10.24425/ather.2024.152002.

Kaczmarczyk T.Z., Ihnatowicz E., Żywica G., Kaniecki M., 2019. Experimental study of the prototype of a Roto-Jet pump for the domestic ORC power plant. *Arch. Thermodyn.*, 40, 33–108. DOI: 10.24425/ather.2019.129995.

Kaczmarczyk T.Z., Żywica G., 2022a. Experimental research of a micropower volumetric expander for domestic applications at constant electrical load. *Sustainable Energy Technol. Assess.*, 49, 101755. DOI: 10.1016/j.seta.2021.101755.

Kaczmarczyk T.Z., Żywica G., 2022b. Experimental study of a 1 kW high-speed ORC microturbogenerator under partial load. *Energy Convers. Manage.*, 272, 116381. DOI: 10.1016/j.enconman.2022.116381.

Kaczmarczyk T.Z., Żywica G., 2024. Experimental study of the effect of load and rotational speed on the electrical power of a high-speed ORC microturbogenerator. *Appl. Therm. Eng.*, 238, 122012. DOI: 10.1016/j.applthermaleng.2023.122012.

Kolasiński P., Daniarta S., 2021. Sizing the thermal energy storage (TES) device for organic Rankine cycle (ORC) power systems. *MATEC Web Conf.*, 345, 00018. DOI: 10.1051/matecconf/202134500018.

Kottapallia A., Konijeti R., 2022. Numerical and experimental investigation of nonlubricated air scroll expander derived from a refrigerant scroll compressor. *Front. Heat Mass Transf.*, 19, 1–11. DOI: 10.5098/hmt.19.11.

Kruk-Gotzman S., Ziółkowski P., Iliev I., Negreanu G.-P., Badur J., 2023. Techno-economic evaluation of combined cycle gas turbine and a diabatic compressed air energy storage integration concept. *Energy*, 266, 126345. DOI: 10.1016/j.energy.2022.126345.

Kupka D., Koloničný J., Pejchal J., 2025. Development of an axial impulse turbine for a small-scale ORC system. *Results Eng.*, 25, 103994. DOI: 10.1016/j.rineng.2025.103994.

Li C., Guo Z., Guo H., Bao X., Zhou L., 2022a. Influences of main design parameters on the aerodynamic performance of a micro-radial inflow turbine. *AIP Adv.,* 12, 105012. DOI: 10.1063/5.0090173.

Li J., Gurgenci H., Guan Z., Li J., Li L., Xue Y., 2022b. Multi-objective optimization of a small scale SCO_2 turbine rotor system with a shaft cooler. *Mech. Ind.*, 23, 21. DOI: 10.1051/meca/2022018.

Li X., Lv D., Liu Y., 2025. Optimization of organic Rankine cycle turbine expander based on radial basis function neural network and nondominated sorting genetic algorithm II. *Phys. Fluids,* 37, 035167. DOI: 10.1063/5.0257260.

Liaw K.L., Kurnia J.C., Lai W.K., Ong K.C., Zar M.A.B.M.A., Muhammad M.F.B., Firmansyah, 2023. Optimization of a novel impulse gas turbine nozzle and blades design utilizing Taguchi method for micro-scale power generation. *Energy*, 282, 129018. DOI: 10.1016/j.energy.2023.129018.

Lu Y., Guo Z., Zheng Z., Wang W., Wang H., Zhou F., Wang X., 2023. Underwater propeller turbine blade redesign based on developed inverse design method for energy performance improvement and cavitation suppression. *Ocean Eng.*, 277, 114315. DOI: 10.1016/j.oceaneng.2023.114315.

Ma C., Yang Q., Sun X., Zhang K., Li L., 2022. Performance analysis of externally pressurized gas journal bearing lubricated with vapor of R134a in centrifugal compressor. *Processes*, 10, 2067. DOI: 10.3390/pr10102067.

Montazerinejad H., Eicker U., 2022. Recent development of heat and power generation using renewable fuels: a comprehensive review. *Renewable Sustainable Energy Rev.*, 165, 112578. DOI: 10.1016/j.rser.2022.112578.

Mukherjee A., Seshadri S., 2023. Numerical study on the effect of port geometry of intake manifold in a steam Wankel expander. *Therm. Sci. Eng. Prog.*, 37, 101621. DOI: 10.1016/j.tsep.2022.101621.

Murthy A.A., Norris S., Subiantoro A., 2022. Performance of a four-intersecting-vane expander in a R134a refrigeration cycle. *Appl. Therm. Eng.*, 209, 118244. DOI: 10.1016/j.applthermaleng.2022.118244.

Peng N., Wang E., Meng F., Zhang W., Wang Y., Zhang B., Zhao Y., Yenga E.C.Y., 2024a. Experimental investigation on off-design performance of a small-scale two-stage counter-rotating impulse turbine. *Int. J. Energy Res.*, 2024, 4623244. DOI: 10.1155/2024/4623244.

Peng N., Wang E., Wang W., 2023. Design and analysis of a 1.5 kW single-stage partial-admission impulse turbine for low-grade energy utilization. *Energy*, 268, 126631. DOI: 10.1016/j.energy.2023.126631.

Peng N., Wang E., Wang W., Lu J., Li M., 2024b. Aerodynamic analysis of a 1.5 kW two-stage counter-rotating partial-admission impulse turbine for small-scale power system with a high expansion pressure ratio. *Case Stud. Therm. Eng.*, 53, 103824. DOI: 10.1016/j.csite.2023.103824.

Pielecha I., Szwajca F., 2024. Experimental study and modelling of an air-cooled proton exchange membrane fuel cell stack in the static and dynamic performance. *Eksploatacja i Niezawodność – Maintenance and Reliability*, 26(2). DOI: 10.17531/ein/184232.

Ping X., Yang F., Zhang H., Wang Y., Lei B., Wu Y., 2022. Performance limits of the single screw expander in organic Rankine cycle with ensemble learning and hyperdimensional evolutionary many-objective optimization algorithm intervention. *Energy*, 245, 123254. DOI: 10.1016/j.energy.2022.123254.

Rusanov R., Kravchenko I., Rusanov A., Riznyk S., Kukhtin Y., Chugay M., Sukhanov M., 2025. Development experience of the centripetal turbine flow part for an aviation engine air starter. *Aerosp. Tech. Technol.,* 1, 38–49. DOI: 10.32620/aktt.2025.1.04.

Sanaye S., Ghaffari A., 2023. Transient modeling and thermal analysis of an innovative dual-loop Rankine–organic Rankine heat recovery system integrated with a gas engine. *J. Therm. Anal. Calorim.*, 148, 10951–10971. DOI: 10.1007/s10973-023-12435-3.

Serafino A., Obert B., Cinnella P., 2023. Multi-fidelity robust design optimization of an ORC turbine for high temperature waste heat recovery. *Energy*, 269, 126538. DOI: 10.1016/j.energy.2022.126538.

Sprouse C.E. III, 2024. Review of organic Rankine cycles for internal combustion engine waste heat recovery: latest decade in review. *Sustainability*, 16, 1924. DOI: 10.3390/su16051924.

Sun H., Li H., Gao P., Hou F., Hung T.-C., Chang Y.-H., Lin C.-W., Qin J., 2024a. Numerical simulation and low speed experiment of a low partially admitted rate axial turbine for small scale organic Rankine cycle. *Appl. Therm. Eng.*, 238, 122002. DOI: 10.1016/j.applthermaleng.2023.122002.

Sun J., Peng B., 2025. Experimental study on the influence of pump frequencies and oil flow rates on the performance of organic rankine cycle systems. *Case Stud. Therm. Eng.*, 69, 106028. DOI: 10.1016/j.csite.2025.106028.

Sun T., Liu Y., Ma Z., Shu P., Ye Z., 2024b. Numerical simulation of the relationship between steam flow excitation characteristics and coverage on the governing stage of marine steam turbine. *Ocean Eng.*, 314, Part 1, 119526. DOI: 10.1016/j.oceaneng.2024.119526.

Tauveron N., Lhermet G., Payebien B., Caney N., Morin F., 2024. An experimental study of an autonomous heat removal system based on an organic Rankine cycle for an advanced nuclear power plant. *Energies*, 17, 5069. DOI: 10.3390/en17205069.

Wang E., Peng N., 2023. A review on the preliminary design of axial and radial turbines for small-scale organic Rankine cycle. *Energies*, 16, 3423. DOI: 10.3390/en16083423.

Weerakoon A.H.S., Assadi M., 2023. Trends and advances in micro gas turbine technology for sustainable energy solutions: a detailed review. *Energy Convers. Manage.: X*, 20, 100483. DOI: 10.1016/j.ecmx.2023.100483.

Weerakoon A.H.S., Assadi M., 2024. Generalized framework for micro gas turbine techno-economic assessment. *Energy Convers. Manage.*, 316, 118820. DOI: 10.1016/j.enconman.2024.118820.

Wei J., Hua Q., Yuan L., Li G., Wang J., Wang J., 2023. A review of the research status of scroll expander. *Proc. Inst. Mech. Eng., Part A: J. Power Energy*, 237, 176–197. DOI: 10.1177/09576509221109245.

Witanowski Ł., 2024. Multi-objective optimization of a small-scale ORC-VCC system using low-GWP refrigerants. *Energies*, 17, 5381. DOI: 10.3390/en17215381.

Witanowski Ł., Klonowicz P., Lampart P., Klimaszewski P., Suchocki T., Jędrzejewski Ł., Zaniewski D., Ziółkowski P., 2023a. Impact of rotor geometry optimization on the off-design ORC turbine performance. *Energy*, 265, 126312. DOI: 10.1016/j.energy.2022.126312.

Witanowski Ł., Klonowicz P., Lampart P., Ziółkowski P., 2023b. Multi-objective optimization of the ORC axial turbine for a waste heat recovery system working in two modes: co-generation and condensation. *Energy*, 264, 126187. DOI: 10.1016/j.energy.2022.126187.

Witanowski Ł., Ziółkowski P., Klonowicz P., Lampart P., 2023c. A hybrid approach to optimization of radial inflow turbine with principal component analysis. *Energy*, 272, 127064. DOI: 10.1016/j.energy.2023.127064.

Włodarski W., Piwowarski M., 2024. A model modification for a microturbine set with partial admission stages. *Energies*, 17, 1792. DOI: 10.3390/en17081792.

Wołowicz M., Kolasiński P., Badyda K., 2021. Modern small and microcogeneration systems – a review. *Energies*, 14, 785. DOI: 10.3390/en14030785.

Wu T., Cai S., Yao Z., Yin X., Ma X., Gao X., Xie F., Yang H., Shen X., Shao L., 2024. Design and optimization of the radial inflow turbogenerator for organic Rankine cycle system based on the genetic algorithm. *Appl. Therm. Eng.*, 253, 123749. DOI: 10.1016/j.applthermaleng.2024.123749.

Zaniewski D., Klimaszewski P., Klonowicz P., Witanowski Ł., Lampart P., Jędrzejewski Ł., Suchocki T., 2023. Organic Rankine cycle turbogenerator cooling – optimization of the generator water jacket heat exchange surface. *Appl. Therm. Eng.*, 223, 120041. DOI: 10.1016/j.applthermaleng.2023.120041.

Zhang H.-H., Zhang Y.-F., Feng Y.-Q., Chang J.-C., Chang C.-W., Xi H., Gong L., Hung T.-C., Li M.-J., 2023a. The parametric analysis on the system behaviors with scroll expanders employed in the ORC system: an experimental comparison. *Energy*, 268, 126713. DOI: 10.1016/j.energy.2023.126713.

Zhang X., Wang X., Cai J., Wang R., Bian X., He Z., Tian H., Shu G., 2023b. Operation strategy of a multi-mode organic Rankine cycle system for waste heat recovery from engine cooling water. *Energy*, 263, Part E, 125934. DOI: 10.1016/j.energy.2022.125934.

Zhang Y., Tsai Y.-C., Ren X., Tuo Z., Wang W., Gong L., Hung T.-C., 2024. Experimental study of the external load characteristics on a micro-scale organic Rankine cycle system. *Energy*, 306, 132453. DOI: 10.1016/j.energy.2024.132453.

Zhang Y., Zhang S., Peng H., Tian Z., Gao W., Yang K., 2023c. Thermodynamic analysis of Tesla turbine in Organic Rankine Cycle under two-phase flow conditions. *Energy Convers. Manage.*, 276, 116477. DOI: 10.1016/j.enconman.2022.116477.

Zhen K., Shi L., Zhang Y., Peng B., 2024. Performance prediction and regression analysis of scroll expander based on response surface methodology. *Case Stud. Therm. Eng.*, 60, 104766. DOI: 10.1016/j.csite.2024.104766.